# Utilization of Multiple Satellite Sensors to Estimate Sea Ice Volume Flux through Fram Strait

G. Spreen, S. Kern, and D. Stammer
*Centre for Marine and Atmospheric Sciences, University of Hamburg, Inst. of Oceanography, Bundesstr. 53, 20146 Hamburg, Germany*

*Keywords:* Sea Ice, Sea Ice Thickness, Remote Sensing, Laser Altimetry

ABSTRACT: The sea ice volume flux through Fram Strait is estimated using a combination of multiple satellite observations. These involve sea ice concentration and drift, combined to yield the area flux, determined from brightness temperature measurements of the 89 GHz channels of the Advanced Microwave Scanning Radiometer (AMSR-E), and estimates of the sea ice thickness distribution, inferred from elevation measurements of the ICESat GLAS instrument. The thickness is derived from ICESat data, by converting its surface elevation measurements into the sea ice freeboard height. Uncertainties in these freeboard height estimates due to geoid model errors are reduced by using the recent geoid from the Arctic Gravity Project (ArcGP). Missing information about the ocean circulation and ocean tides is approximated locally by interpolating the sea surface height linearly between leads for every ICESat orbit. This approach is evaluated using coincident Synthetic Aperture Radar imagery. The average freeboard height distribution is calculated for complete ICESat measurement periods using a standard polar-stereographic grid. Using typical average values for ice density and snow depth and density derived from a climatology in combination with in situ measurements, the freeboard height is converted into an average ice thickness distribution. Sea ice area flux and thickness are combined to get an estimate of the sea ice volume flux through Fram Strait. The meridional ice volume flux estimated for 79°N amounts to 168 km³ and 62 km³ for the Feb/Mar and Oct/Nov ICESat measurement periods in 2003, respectively, with a relative error of at least 20%. These values lie in the absolute range given by previous similar studies, but are considerably smaller than the average ice flux during the 1990s. There is evidence that this is caused by a smaller ice drift speed during 2003 compared to the 1990s – particularly during the autumn measurement period.

## 1 INTRODUCTION

Changes in the mass balance of Arctic sea ice have been shown to influence the global climate in various ways (Bamber and Payne, 2004). With respect to the ocean changes in the amount and location of the release of freshwater and brine are two of the most important.

Two main processes can be identified for a change in Arctic sea ice mass: a change in the net amount of sea ice production and in the export of sea ice out of the Arctic Ocean. The first process depends on the length of the freezing period, snow accumulation, ice production in polynyas and meteorological conditions. The second process is largely determined by the sea ice export through Fram Strait into the Greenland Sea, since export through Fram Strait is by far the largest portion of the total Arctic sea ice export. Currently the net annual sea ice volume exported through Fram Strait amounts to about 10% of the total sea ice volume of the Arctic Ocean and is the single largest source of freshwater in the Greenland-Icelandic-Norwegian (GIN) Sea (Aagaard and Carmack, 1989). Anomalies in this export are major contributors to the freshening of surface waters in the Greenland and Labrador Seas and by this may enhance or hamper convective overturning and water mass modification. This in turn can result in significant changes in the export of dense water from the GIN Sea into the Atlantic Ocean and then impact the global ocean thermohaline circulation (Dickson et al., 1988; Karstensen et al., 2005).

While in sea ice model studies the ice volume or ice mass flux is one of the quantities of the most interest, it is difficult to get this flux from observations. Sea ice area and motion, ice thickness and ice density have to be known to derive the sea ice volume flux, and is not possible to obtain these with

any one measurement technique. A multi sensor approach has therefore been chosen by other groups (e.g. Kwok et al., 2004a) and is also chosen for this study, with the goal to utilise only satellite measurements. The sea ice area and motion are measured routinely, daily (area) or every other day (motion), and globally, based on all-weather and daylight independent space-borne passive and/or active microwave sensors like the Special Sensor Microwave/Imager (SSM/I) or the SeaWinds QuikSCAT since late 1978 (e.g. Agnew et al., 1997; Kwok et al., 1998; Cavalieri et al., 2002). It became evident from this data that the sea ice extent of the Arctic Ocean is currently shrinking (Cavalieri et al., 2003). It is expected to further decrease in response to accelerated Arctic climate warming (Johannessen et al., 2004). Here we use data from the Advanced Microwave Scanning Radiometer (AMSR-E) to obtain sea ice concentration and motion.

More crucial for the volume flux determination is the sea ice thickness measurement at a similar scale to the ice area measurements. Until recently, our knowledge of the sea ice thickness distribution in the polar regions was merely based on in-situ drillings, ice draft observations by upward looking sonar (ULS), and ground-based and airborne electromagnetic sounding (e.g. Wadhams, 2002, Haas, 2004). Such measurements have been used to infer the sea ice volume flux through Fram Strait with the limitation that the sea ice thickness across the Fram Strait has to be extrapolated from one point measurement. Laxon et al. (2003) were the first to publish at least an average sea ice thickness distribution of the Arctic Ocean derived from satellite radar altimetry. The averaging period, however, is too long to use this data to derive the sea ice volume flux. Nevertheless, these data sources reveal that the Arctic sea ice seems to have thinned substantially since the late 1950s (Rothrock et al., 2003 and 1999; Wadhams and Davis, 2000; Haas, 2004). Together with the shrinking ice area, this means a significant reduction of the Arctic sea ice volume. Whether this reduction will continue towards an ice free Arctic Ocean in the future, or whether the downward trend can be attributed to a multi-decadal oscillation (e.g. Divine and Dick, 2006), which will reverse into an upward trend in the future, has to be carefully monitored.

ICESat's (Ice, Cloud, and land Elevation Satellite) Geoscience Laser Altimeter System (GLAS) is the first space-borne instrument, which at least comes close to the needed spatial and temporal resolutions needed to monitor the sea ice thickness globally. Unfortunately this mission only started in 2003 and, due to a hardware malfunction, GLAS is only operating for up to three periods of about one month duration per year. Thus currently ICESat data cannot be used to make long-term estimates of the sea ice thickness variability, as the time series is interrupted and too short. Despite these limitations, we demonstrate that ICESat data can be used, in combination with other satellite data, to estimate the sea ice volume flux independently from in-situ measurements. Thus in the future, when the time series is longer and/or more sensors are measuring similar quantities, the sea ice volume flux can be estimated at least on a monthly scale globally.

We focus on Fram Strait sea ice volume flux. This is highly variable, e.g. Kwok et al. (2004a), and its amount is determined by the sea ice thickness at the northern entrance of the Fram Strait and the wind forcing. It was shown by Pfirman et al. (2004) that sea ice export through Fram Strait can occur in surge-like events, where large portions of the old, thick ice leave the Arctic Ocean. Depending on the strength and location of the Beaufort Gyre and the Transpolar Drift, it takes several years until ice of similar thickness has formed again. Estimates of Fram Strait sea ice volume flux (1970s to 1990s) range from 1600 $km^3$/year to 5000 $km^3$/year. During 1991-1999, averaged transports amount to (2218 ± 497) $km^3$/year (Kwok et al., 2004a). These estimates were obtained primarily using ULS data by extrapolating local thickness estimates across the entire Fram Strait to obtain a complete cross-strait ice thickness profile (e.g. Vinje et al., 1998). In this study, this cross-strait profile is measured by ICESat's GLAS, which measures its height above the Earth's surface, from which the sea surface height (SSH) and the sea ice freeboard height (called freeboard hereafter) can be inferred. Kwok et al. (2004b) provide a first estimate of the sea ice thickness distribution from ICESat data from selected satellite overpasses. Key problems are i) inaccurate sea surface height (SSH) estimates, ii) unknown snow depth and ice density, which are needed to convert freeboard to ice thickness, iii) contamination by clouds. Therefore, best results are expected to be obtained in regions with a stationary sea ice cover, which permits averaging over long/large periods/areas. These conditions are not met in the Fram Strait/Greenland Sea: sea ice is known to drift several kilometres per day, divergence and convergence

can continuously change surface roughness, and snow accumulation can be very variable, and therefore careful error estimates are crucial to determine the reliability and accuracy of the estimated quantities – like sea ice freeboard height and volume flux.

In this study present state-of-the-art AMSR-E distributions of sea ice concentration (area) and motion are combined with sea ice thickness distributions of two GLAS measurement periods in the Fram Strait region, to obtain the sea ice volume flux distribution.

## 2 DATA, CONCEPTS AND METHODS

For our estimates of sea ice volume flux, satellite information about sea ice area, its drift and thickness have to be combined (see Figure 1). Other information from in-situ and airborne sources are only used

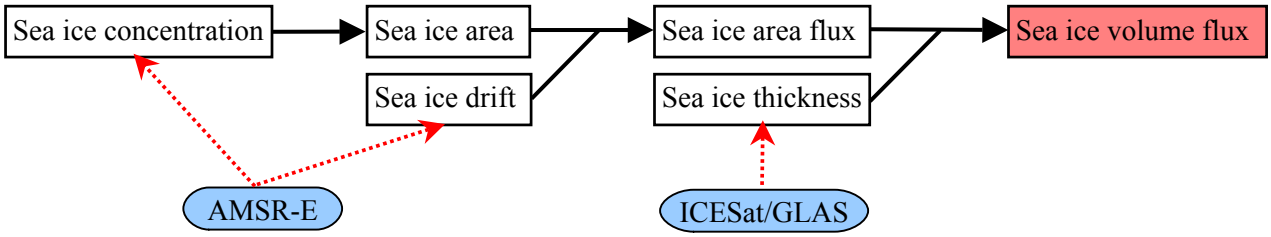


Figure 1: Schematic flow diagram of quantities (black boxes) and satellite sensors (blue ovals) involved in the estimation of the sea ice volume flux.

indirectly, e.g., as geoid model and as *a priori* information on sea ice density and as snow depth and density. All data are interpolated on a polar stereographic 25 km grid covering the Fram Strait region (e.g. Figure 3). Data sets are explained from left to right in Figure 1:

### 2.1 SEA ICE CONCENTRATION AND AREA

Sea ice concentration gives the percentage of a defined area, here the grid cell, covered with sea ice. By multiplying the sea ice concentration with the grid cell area the sea ice area per grid cell is obtained. We use data obtained by the Advanced Microwave Scanning Radiometer for EOS (AMSR-E) on board NASA's AQUA satellite. It measures the thermal radiation of the earth at 6 different microwave frequencies (7, 11, 19, 24, 37 and 89 GHz) at horizontal and vertical polarization. These microwave measurements are, in contrast to visual and infrared ones, almost independent of daylight and clouds. The Arctic region is completely covered each day at least once.

Sea ice concentrations are calculated with the ARTIST Sea Ice (ASI) algorithm (Spreen et al., 2005b; Kaleschke et al., 2001). It uses the 89 GHz channels, which offer the highest spatial resolution (~5 km) of all channels but are hampered slightly more by the water vapour and cloud liquid water in the atmosphere. A combination of the 19, 24 and 37 GHz channels are used to eliminate this atmospheric influence over the open ocean off the ice edge which otherwise may cause spurious ice concentrations. An example of ice concentration in the study region for February 26, 2003, is shown in Figure 2. Clearly, this ice concentration map shows the variable ice conditions typical for the Fram Strait during winter, with regions of a very compact but also a quite open ice cover along the ice edge. Moreover, the fine spatial resolution allows resolution of smaller scale features such as polynyas along the coast or downstream of huge multi-year ice floes, as well as the disintegration of the ice pack into ice patches and fingers in the marginal ice zone (MIZ) (see black box). The ice concentrations are sampled down onto the 25 km grid used for the final sea ice volume flux estimates. An example of this smoothed ice concentration data is shown as background in Figure 3 for the same day as Figure 2.

## 2.2 SEA ICE DRIFT AND SEA ICE AREA FLUX

Sea ice drift can be obtained from satellite passive microwave radiometry by the cross-correlation of fields of time-lagged data (e.g. Kwok et al., 1998) in which recognizable features are tracked. As these features have to be correlated the already coarse resolution of passive microwave sensors is further reduced. We again use the 89 GHz channel data of AMSR-E, which currently offer the highest spatial resolution for passive microwave remote sensing. The French Research Institute for Exploitation of the Sea (IFREMER) provides a daily data set of ice drift on 31.25 km grid using AMSR-E data with a time gap of two days (Ezraty et al., 2005). Ice drift is calculated separately for the vertically and horizontally polarized 89 GHz daily brightness temperature maps on a 6.25 km grid. The Laplacian motion of 5 x 5 pixel fields (31.25 x 31.25 km2) are calculated using a maximum correlation technique. Finally, the two derived drift vector maps (from horizontally and vertically polarized data) are merged to one consistent ice drift field. The error in ice drift speed is estimated by comparison to ice drift speeds from the International Arctic Buoy Program (IABP) and was 2.6 cm/s (2.2 km/day) for the complete Arctic (Ezraty et al., 2005). However, the error is expected to be larger in dynamic regions such as the Fram Strait. We interpolate the 31.25 km grid fields onto our 25 km grid. An example for the ice drift on February 26, 2003, is shown in Figure 3. In a small band east of Svalbard a strong outflow of sea ice is taking place. In the Fram Strait the ice motion increases from west to east. By multiplying the sea ice area of section 2.1 with the sea ice drift the sea ice area flux is determined.

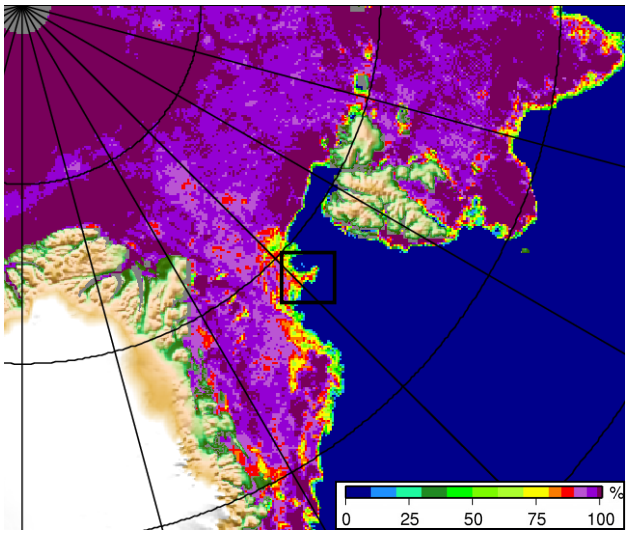


Figure 2: Sea ice concentration on 26 February 2003 in Fram Strait region obtained from AMSR-E 89 GHz data (ARTIST Sea Ice (ASI) algorithm). Grid spacing is 6.25 km. The corresponding sea ice drift is shown in Figure 3.

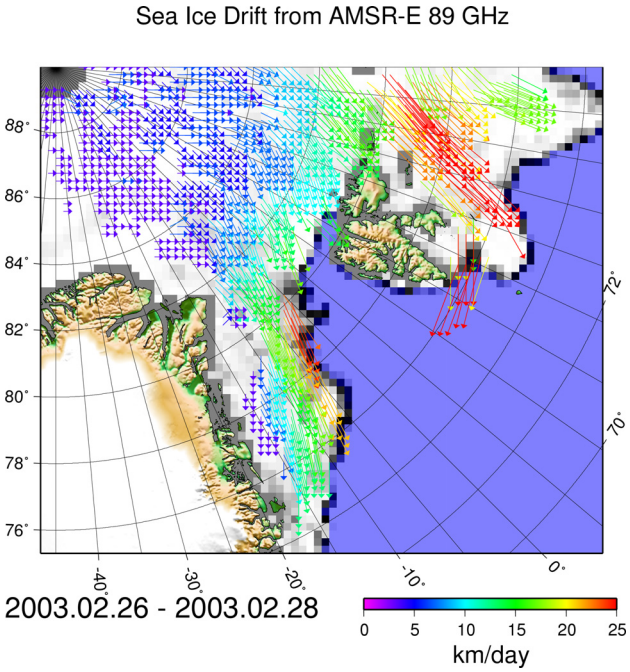


Figure 3: Two-day gap colour-coded sea ice drift in Fram Strait region obtained from merged vertically and horizontally polarised AMSR-E 89 GHz data. 26-28 February 2003; grid spacing is 25 km (interpolated from 31.25 km grid). Background: ASI sea ice concentration, see Figure 2 for details.

## 2.3 SEA ICE FREEBOARD

As a prerequisite step to obtain the sea ice thickness the sea ice freeboard is determined. The GLAS instrument aboard ICESat permits observation of the sea ice up to 86° North. Here GLAS data for the first two ICESat measuring periods 20 February to 19 March 2003 (period I) and 26 September to 17 November 2003 (period II) is used (GLA13 datasets).

By measuring twice the laser pulse travel time at 1064 nm wavelength between the sensor and the surface, the height of the sensor, $D_{laser}$, above the surface is obtained for a footprint of 64 m diameter every 170 m along track (see Fig. 4 and Zwally et al., 2002). ICESat's orbit and thus its height above a

reference ellipsoid, $h_{ellip}$, is determined with an accuracy of 5 cm. By subtracting $D_{laser}$ from $h_{ellip}$ the mean surface elevation in the footprint above the reference ellipsoid is obtained. After atmospheric and tidal corrections the total error budget for a single ICESat surface elevation measurement was estimated as 13.8 cm (Zwally et al., 2002). By subtracting the geoid height, $h_{geoid}$, and the contribution to SSH due to the ocean dynamics, $\Delta h$, an estimate of the sea ice freeboard height, F, can be obtained (see Figure 4). $\Delta h$ contains contributions caused by ocean currents, steric SSH changes, atmospheric pressure loading, and ocean and Earth tides. Accordingly, the ice freeboard $F$ is given as

$$F = h_{ellip} - D_{laser} - SSH = h_{ellip} - D_{laser} - h_{geoid} - \Delta h. \quad (1)$$

Similar to all altimeter studies, an accurate geoid is a necessary prerequisite to estimate the ice freeboard. In a preliminary study, Spreen et al. (2005a) found that using the project-provided geoid (EGM96), causes unrealistically large variations of the SSH (several metres) in some regions of the Greenland Sea. We therefore use a more recent gravity field compiled by the Arctic Gravity Project (ArcGP). It represents today's best geoid north of 64° latitude and combines gravity data from several airborne surveys, surface measurements (ground, helicopter, marine), submarine data, satellite altimetry and GRACE (Gravity Recovery and Climate Experiment) data on a 5'x5' grid (Forsberg and Kenyon, 2004; Forsberg and Skourup, 2005). Figure 5 demonstrates the significant improvement of the ArcGP geoid in comparison to the EGM96 geoid. In the Fram Strait differences of ±4 m between the two geoid

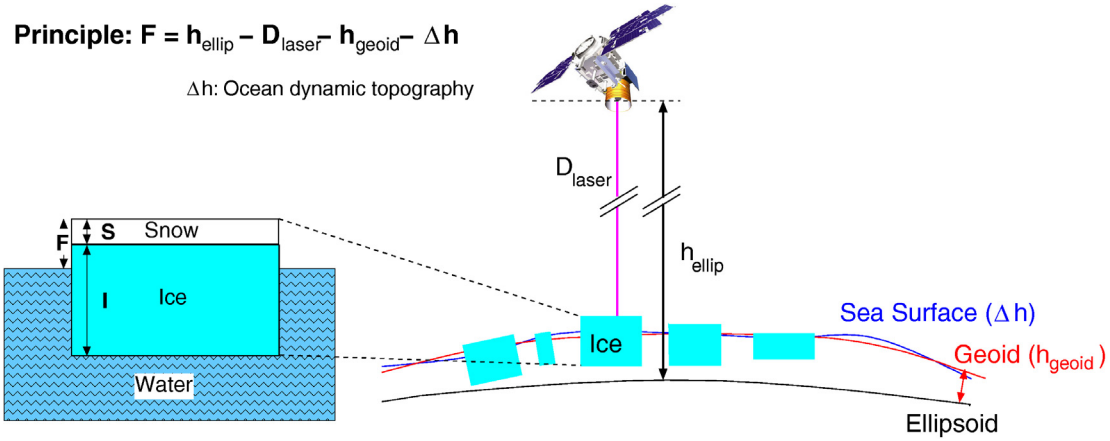


Figure 4: Schematic diagrams showing the interrelation of ice freeboard, *F*, snow depth, *S*, and sea ice thickness, *I* (left) and an artist's view of ICESat above the three involved surfaces: reference ellipsoid, geoid, and sea surface (right).

models become apparent which compares well to the above mentioned discrepancies in the SSH (Spreen et al., 2005a). For our purposes, the ArcGP geoid heights are interpolated bi-linearly onto the locations of the ICESat measurements before they were subtracted from the surface elevation data. As explained in Figure 4, the dynamic part, $\Delta h$, of the ocean has to be removed next from the remaining SSH field before an estimate of the ice freeboard can be obtained. No measurements or models exist to date, which would provide an accurate estimate of the dynamic SSH field during period I and II. Instead, $\Delta h$ has to be inferred from the ICESat data itself. For that purpose we use the "lowest level elevation method" proposed by Zwally and Yi (personal communication, 1st CryoSat Workshop, 2005, http://earth.esa.int/workshops/cryosat2005/, and IGARSS'05, July 25-29, Seoul, Korea) to get the absolute ice freeboard estimates. A similar method was used for airborne laser measurements by Hvidegård and Forsberg (2002) and recently adopted for ICESat data (Forsberg and Skourup, 2005).

We adapted this method for our purpose as follows:

(1) We divided the daily GLA13 dataset into separate ICESat overpasses and took only elevation measurements with positive data-quality flags, and an uncorrected reflectivity between 0.1 and 0.9. Additionally we removed outliers and spikes by filtering.

(2) We removed elevation data which were located in open water by using sea ice concentrations calculated from AMSR-E data with the ASI algorithm described before. Elevations in areas with zero

ice concentration are excluded from further analysis.

(3) We filtered out the large-scale dynamic variability of the SSH by smoothing the remaining elevations with a 50 km boxcar running mean and subtracting the smoothed from the original elevations. The lowest 2% of the data points in these residual minimum elevations are identified and assumed to represent areas of open water or young, thin ice. This assumption is reasonable, because such areas (leads) are abundant in the study region (sea ice concentrations calculated on a 25 km x 25 km grid rarely exceed 98%), and the combination of the frequent sampling (every 170 m along track) and the small footprint size (64 m) of the GLAS ensures that several leads are hit during one ICESat overpass. It should be mentioned that this 2%-rule certainly results in an underestimation of open water areas in the MIZ.

(4) We fit the remaining minima linearly using a least absolute deviation method to account for remaining trends in the elevations after boxcar averaging.

(5) The derived SSH was subtracted from the measured elevations to obtain the ice freeboard.

An example for a part of one orbit on 23 February 2003 demonstrating how this method works is shown in Figure 6. The black lines are the GLAS elevations after filtering with the 50 km running mean. The blue line connects the lowest 2% of data points. In red the finally fitted SSH is given. Subtracting the red line from the black elevation and setting all remaining negative values to zero yields the required sea ice freeboard height.

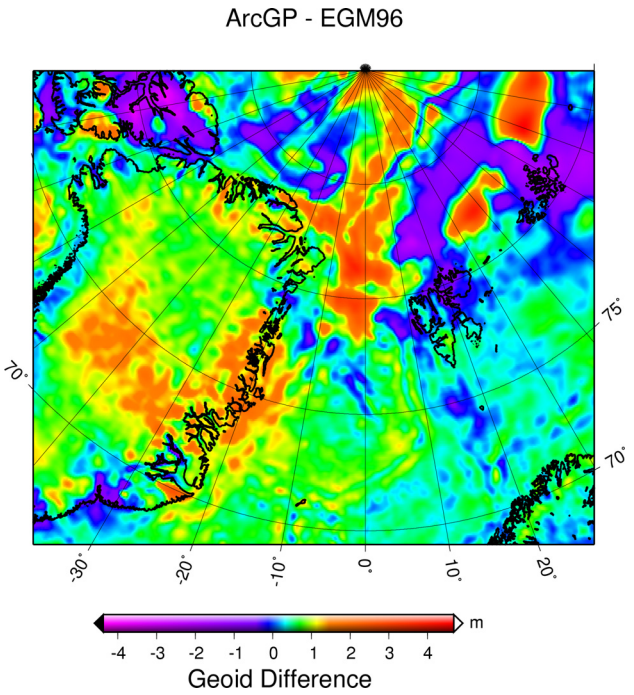


Figure 5: Difference between the more accurate ArcGP and ICESat's standard EGM96 geoid. Differences of ±4 m can be observed in the Fram Strait region.

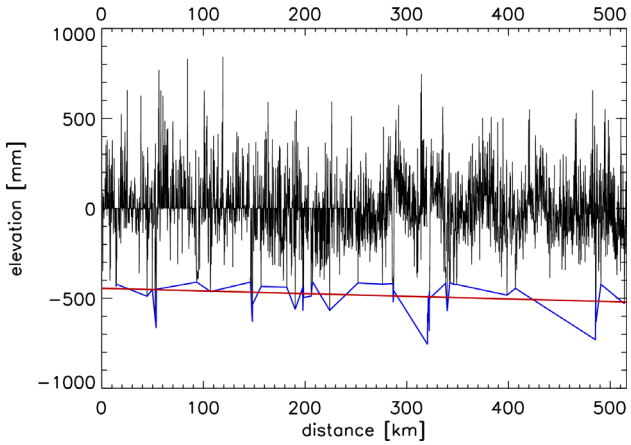


Figure 6: Example from 23 February 2003 showing the principle of the lowest level elevation method. Black: high-pass filtered GLAS elevations, blue: connected lowest 2% of elevation data; red: the resulting SSH.

Following this approach, the ice freeboard distribution is calculated on a 25 km grid as a mean of all overpasses for period I (Feb/Mar 2003) and II (Oct/Nov 2003), yielding a mean value of 55 ± 18 cm for period I and of 34 ± 19 cm for period II, respectively. The stated ± bands describe the variability of the ice freeboard in our study region.

To check if the lowest level elevation method works properly, we compared several Envisat ASAR scenes with our ICESat freeboard heights on a single orbit base. One example of this comparison is shown in Figure 7. In a typical winter-time SAR image of the Arctic Ocean sea ice cover the radar backscatter takes high values (grey-white in Figure 7) over multiyear ice and low values (black-dark grey in Figure 7) over smooth first-year ice, young ice and calm open water. In Figure 7 some of these dark regions are marked with red circles. The overlaid GLAS freeboard heights drop to near zero

exactly in this region. The remaining shift in the location of the open water/thin ice areas identified between both datasets can be ascribed to the ice drift during the acquisition time difference of the two data sets. This difference causes the biggest problem for comparison of these datasets. If the time difference exceeds 2-3 hours in most cases no agreement between both datasets can be found; otherwise the match between these datasets in general is comparable to the example shown here. Additional problems might be caused by an inaccurate geo-location of the datasets. However, overall the comparison showed good agreement, underlining the feasibility of our approach.

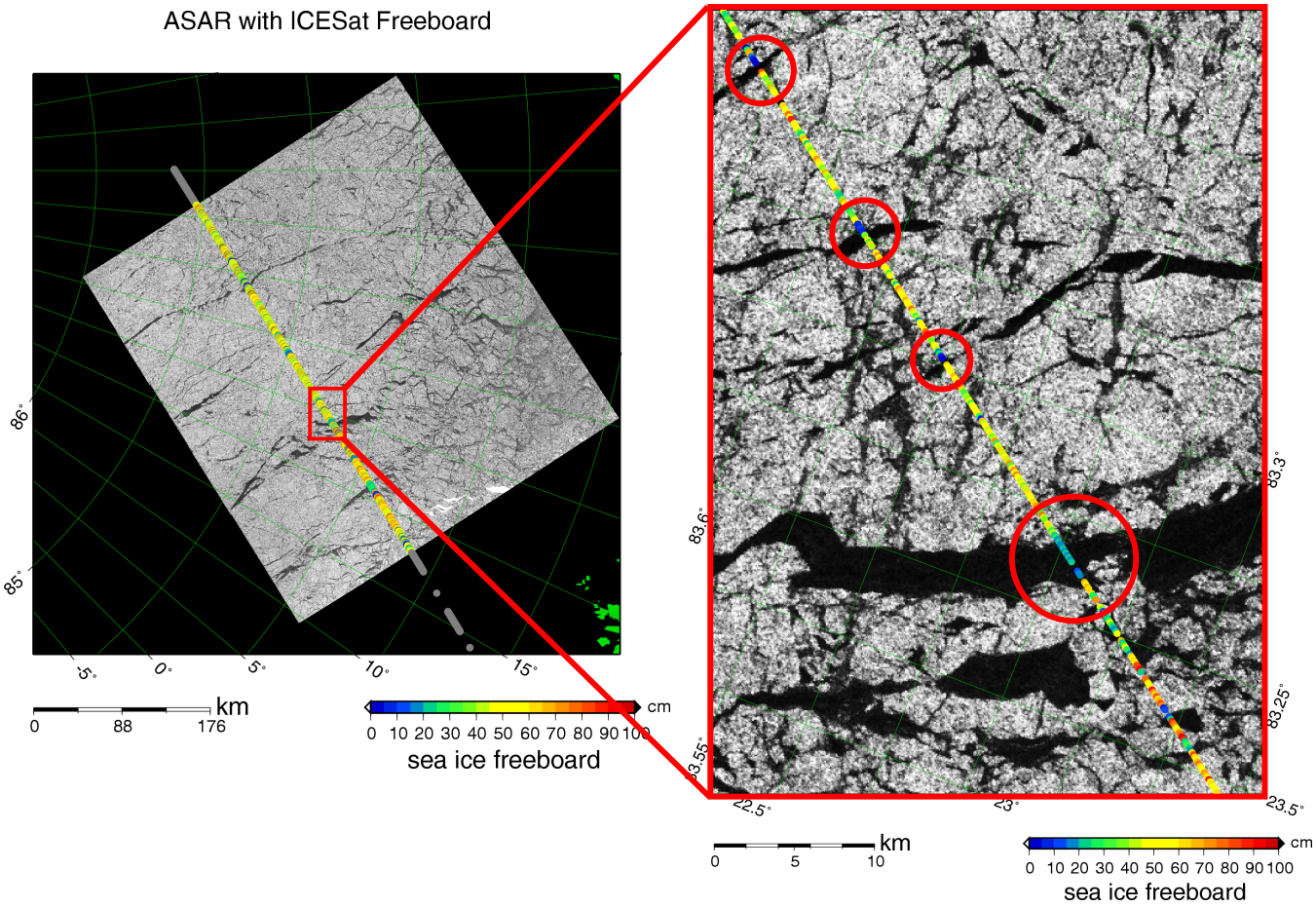


Figure 7: Envisat ASAR image from 09 March 2003, 16:52 UTC, overlaid by colour-coded GLAS sea ice freeboard heights (not to scale) of an ICESat overflight of the same day, 15:41 UTC. Left: complete 400 km x 400 km wide-swath ASAR scene north of Svalbard; right: zoom of the part enclosed by the red rectangle. Red circles mark regions where the SAR image shows leads (covered either by smooth first-year ice and/or thin ice and/or calm open water) and accordingly the ICESat freeboard drops down to values near zero. A slight shift in the location of the leads in the two datasets can be attributed to the ice drift during the 1:10 hour time difference.

## 2.4 SEA ICE THICKNESS

To retrieve ice thickness, $I$, from the ice freeboard, $F$, prior information about snow thickness, $S$, and the densities of ice, $\rho_I$, of snow, $\rho_S$, and of water, $\rho_W$, has to be known (see Figure 4). Because no reliable satellite snow depth measurements are available covering our study region and period, we used in-situ snow depth and density measurements available in the vicinity of our study area in combination with a snow climatology. Snow thickness, and snow and ice density measurements from R/V "Polarstern", which operated in April 2003, one month after period I, north of Svalbard, are taken as reference for period I. The observed mean snow thickness, $S$, was 20 cm (range: 0 – 70 cm) with a density, $\rho_S$, of 330 kg/m$^3$. The mean ice density, $\rho_I$, was 850 kg/m$^3$ (range: 825 – 890 kg/m$^3$). Here the upper limit of $\rho_I$ = 890 kg/m$^3$ is taken in order to account for the considerable fraction of first-year ice in the study area, which is not represented properly by these ice density measurements, of predominantly multi-year ice. Isostatic balance is assumed (on average), i.e. the snow depth on freely floating ice has to be always less

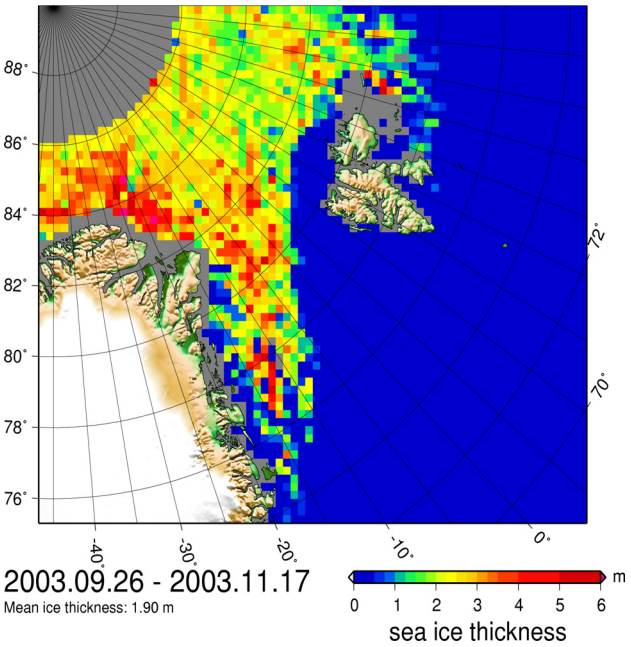


Figure 9: Mean sea ice thickness derived from ICESat GLAS observations for Oct./Nov. 2003 (ICESat measurement period II). Grey areas denote missing data

than or equal to the ice freeboard. For thin ice the snow depth is therefore reduced. With these parameters the ice thickness $I$ for period I can be calculated from the ice freeboard $F$ according to Archimedes' principle as:

$$I = F\frac{\rho_W}{\rho_W - \rho_I} + S\frac{\rho_S - \rho_W}{\rho_W - \rho_I} = 7.65F - 5.18S. \quad (2)$$

For period II, snow parameters can be expected to substantially differ from those of period I (e.g. Warren et al., 1999). In-situ measurements representative of snow conditions during period II are not available. Alternatively climatological snow depths (Warren et al., 1999) could be used, revealing values in the range of 19 cm and 32 cm for October and March (resemble period II and I) for the complete Arctic, respectively. However, these values are based on observations made during 1954 to 1991 predominantly in the central Arctic. Meanwhile the ice age and thickness and presumably also the snow depth have changed but most likely not the seasonal cycle, i.e. the ratio between spring and autumn snow depths should be the same. Therefore, we estimated the snow depth of period II, by taking the snow depth $S$ measured during spring as reference, as $S = 19/32*0.2$ m = 0.12 m. After Warren et al. (1999) the snow density in the Arctic varies seasonally rather than spatially so that their snow density estimate for October/November of $\rho_S = 280$ kg/m$^3$ is taken for period II. This is supported by their snow density measurements of 325 kg/m$^3$ for March/April, which match well with the measurements during CryoVEx of 330 kg/m$^3$. This leads to estimates of the ice thickness during period II as:

$$I = 7.65F - 5.56S. \quad (3)$$

The sea ice thickness distribution as derived from the GLAS ice freeboard estimates (Figure 8) using equation (3) for ICESat period II (Oct/Nov) is shown in Figure 9. They are scaled with ASI sea ice concentrations (section 2.1) sampled onto the 25 km grid. Thus the given thickness is the mean sea ice thickness in the corresponding grid cell, including the open water part. The mean sea ice thickness amounts to 3.0 m and 1.9 m, during periods I and II, respectively. The mean error budget of every grid cell is quite large and of the order of 1 m for both periods using conservative error assumptions for the individual variables. A more detailed error discussion can be found in Spreen et al. (2006).

## 2.5 SEA ICE VOLUME FLUX

Finally the sea ice volume flux out of every grid cell was obtained by combining sea ice area flux

(section 2.2) with the sea ice thickness estimates derived from ICESat data. The sea ice volume flux $Vf$ is calculated by multiplying the sea ice thickness $I$ of every grid cell with the grid size $G$ and the absolute value of the sea ice motion $M$ of this cell:

$$Vf = I \cdot G \cdot M. \quad (4)$$

The spatial distribution, mean amount and direction of the sea ice volume flux estimated with equation (4) using the AMSR-E drift is shown for the Fram Strait region for autumn periods II in Figure 10. The zonal distribution of the meridional volume flux through a transect at 79°N (marked with a black line in the main panel of Figure 10) is shown in the inset of Figure 10.

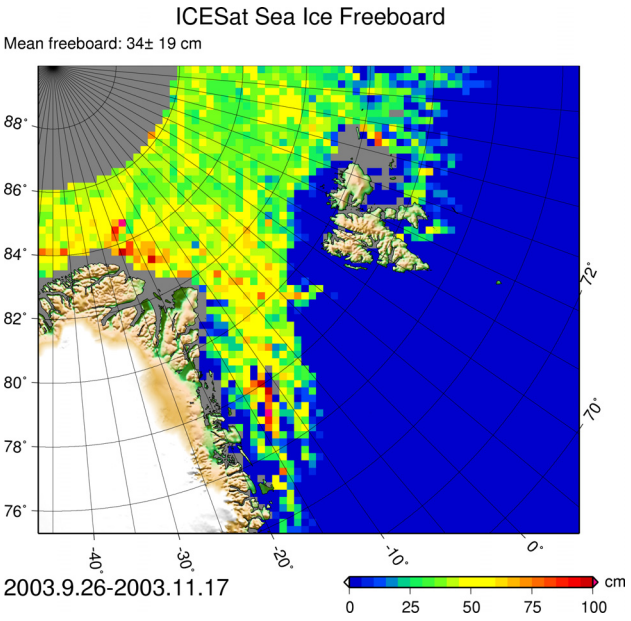


Figure 8: Sea ice freeboard height distribution derived from GLAS elevation data for the second ICESat measurement period in autumn 2003. All data of this 53 days period are averaged on a 25 km grid. Grey areas mark missing data.

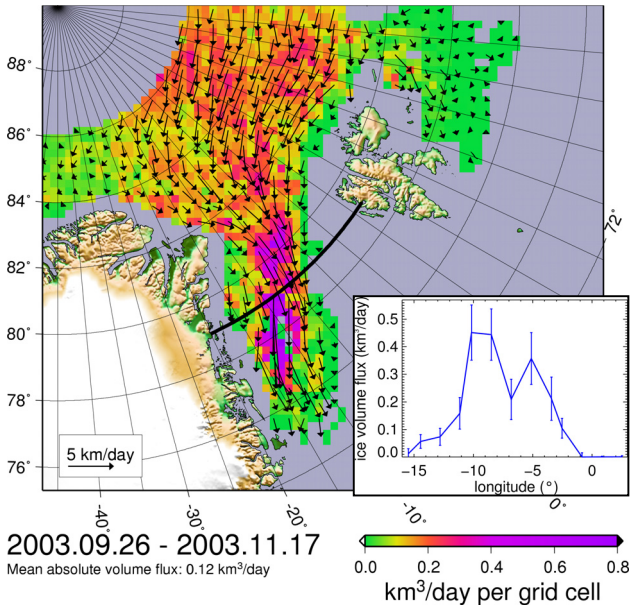


Figure 10: Main: Sea ice volume flux in the direction indicated by the ice motion vectors (AMSR-E ice drift, starting at every third grid cell) for Oct./Nov. 2003 (ICESat period II). Grid cells with either or both no ICESat or no AMSR-E data are marked gray. Inlay: Zonal distribution of the meridional sea ice volume flux across transect at 79°N (black line in main panel). Error bars denote the RMS error budget of the transect data points.

## 3 RESULTS AND DISCUSSION

The spatial distribution of sea ice volume flux has been obtained from solely satellite observations. For such estimates, sea ice parameters, obtained from various satellites, have to be combined. Figure 10 represents the mean daily flow of ice volume for every grid cell in the direction of the AMSR-E based ice drift vectors during ICESat measurement period II. Analogous results were obtained for ICESat measurement period I (not shown here). Inflow from neighbouring grid cells is not considered. The figure clearly suggest that the ice volume flux through Fram Strait is not evenly distributed across the strait, but strongly concentrated toward its western portion. Near Greenland, thick, land-fast ice prevails. Accordingly, its ice motion and volume fluxes tend to be negligible. However, east of this region the volume flux reaches its highest values, coincident with the East Greenland Current (EGC) axis, which supports the transport of thick multi-year ice from the Fram Strait southward. Further eastward, the flux values decline towards the open water area. The mean ice thickness in period II is about 1 m smaller than in period I (1.9 m to 3 m). This can be explained to some extent by the thinning of ice through melting during summer months. Moreover, the ice drift distribution suggests that the ice in the Fram Strait region and the EGC during period I originates from a thick-ice region north of Greenland, while during period II the ice flux tends to originate from the transpolar drift with smaller ice thickness. The

sea ice drift of period I appears, on average, about twice what is shown for period II.

The meridional ice volume flux across 79°N latitude for period I is displayed in the inlay of Figure 10. To calculate this meridional flux, data from three grid points around these latitudes (approximately one north, one at the latitude and one south) have been averaged. Also shown as error bars are the root mean square (RMS) values of the flux calculated by error propagation (details in Spreen et al., 2006). The ice volume flux is maximum between -10° and -7°E. Calculating the total flux through the transect at 79° N gives 5.6 ± 1.0 km3/day for period I and 2.1 ± 0.4 km3/day for period II. From these values the monthly (30 days) volume fluxes result in 168 ± 31 km3 and 62 ± 13 km3, respectively.

Compared to the Fram Strait mean volume flux estimates of Kwok et al. (2004a) and Vinje et al. (1998) given for the 1990s, our estimates are small. Both studies used a combination of ice drift estimates from satellite microwave radiometry (SSM/I), together with ice thickness estimates obtained from ice draft measurements by ULS at near 79°N, 5°W. Their mean volume flux estimates in the 1990s averaged ~340 km3 for March and ~230 km3 for October in comparison to our one year estimates of 168 ± 31 km3 and 62 ± 13 km3 for 2003. Assuming that both datasets are comparable, both periods, but especially the second ICESat measurement period, showed lesser sea ice volume fluxes compared to the 1990s. Such low volume fluxes did occur in the 1990s, however, the minimum values reported by Kwok et al. (2004a) and Vinje et al. (1998) for the two months February/March and October/November are 94 km3/month and -2 km3/month, respectively. Therefore our estimates lie in the range of previously calculated values. Our relative uncertainty for the total ice volume flux through the 79°N transect is around 18% and comparable to the uncertainties of 12% to 20% published by Vinje et al. (1998) for their method.

It would have been nice to use their method also during the ICESat measurement periods to compare our results, but unfortunately the ULS time series distributed by the National Snow and Ice Data Centre (NSIDC) stops in 2002 before the ICESat launch. Data we have got from other institutions, which operate ULS instruments, e.g. the Norwegian Polar Institute (NPI) in Tromsø (Edmond Hansen, personal communication, 2005), also stop in 2001.

The largest part of the volume flux variability is caused by the variability of the ice drift. We therefore compared the ice drift used in our study to the mean ice drift for the corresponding months of the years 1991 to 2002 (Kwok et al., 2004a) at a zonal flux gate at 80°N. The maximum ice drift values along the gate for ICESat period I are more than 15% smaller than the corresponding mean drift values for 1991 to 2002. The zonal drift distribution is also much narrower. For ICESat period II (Oct./Nov.) the AMSR-E derived maximum ice drift values are more than 50% smaller than for October 1991–2002. This is a strong argument towards an extraordinary small ice volume flux during ICESat period II compared to previous years, which would explain our smaller result.

## 4 CONCLUSIONS

We presented here a multi-sensor satellite approach to estimating the sea ice volume flux, which allows - for the first time - calculations of the spatial distribution of this flux on a monthly basis. The approach combines surface elevation measurements obtained by the ICESat GLAS instrument with the sea ice area flux (combination of sea ice concentration and drift) obtained from brightness temperature measurements of the 89 GHz channels of the Advanced Microwave Scanning Radiometer (AMSR-E). The thickness is derived from ICESat data by converting its surface elevation measurements into the sea ice freeboard height. Using the recent geoid from the Arctic Gravity Project reduces uncertainties in these freeboard height estimates due to geoid model errors. Missing information about the ocean circulation and ocean tides is approximated locally by interpolating the sea surface height linearly between leads for every ICESat orbit. The average freeboard height distribution is calculated for single ICESat measurement periods using a standard polar-stereographic grid. Using typical average values for ice density and snow depth and density derived from a climatological dataset in combination with in-situ measurements, the freeboard height is converted into an average ice thickness distribution. Sea ice area flux and thickness are finally combined to get an estimate of the sea ice volume flux. The approach is applied to data of the first two ICESat measurement periods (Feb./Mar., period I, and Oct./Nov., period

II, 2003) in the Fram Strait region. Estimated meridional ice volume fluxes across 79°N amount to approximately 170 km³ and 60 km³ for period I and II, respectively, with a relative error of about 20%. One reason for the fact that these values are at the lower bound of earlier observations during the 1990s using ULS-derived ice thickness, particularly for period II is certainly the significantly smaller ice drift speed observed during period II as compared to the 1990s. However, because of a large inter-annual variability in the ice drift, a direct comparison between our results and those of earlier studies is not meaningful.

The parameters sea surface height (SSH), ice density, snow density and depth, and ice drift, which determine the accuracy of our ice volume flux estimates, are highly variable and/or cannot be determined with sufficient accuracy. An error and sensitivity analysis (Spreen et al., 2006) reveals that SSH, ice drift speed, snow depth, and ice density can be of equal importance for the accuracy of the ice volume flux. Regarding SSH, improved estimates can be expected from a more accurate geoid and improved information about day-to-day variations in dynamic ocean surface topography, which together could allow a more accurate estimation of the ice freeboard height. Ice drift speed estimates could be improved by using an approach especially tuned for the highly dynamic Fram Strait region, e.g. an approach which is less vulnerable to the atmospheric influence, and which allows a finer spatial resolution. The usage of Synthetic Aperture Radar (SAR) data could be an alternative (Kwok et al., 2004a). A further validation and/or enhancement of the AMSR-E snow depth algorithm for Arctic sea ice (Comiso et al., 2003) would be required to use its results for our goals. At the time of writing the snow depth estimates available from AMSR-E data for the Fram Strait region are significantly smaller than corresponding in-situ measurements and are thus not used in this study. Most difficult would be an improvement with respect to the ice density, which could be achieved, however, by distinguishing at least first- and multi-year ice, and assigning different density values for each class when converting the freeboard heights into ice thickness.

Unfortunately, ICESat is only operating 3 months a year at maximum. Therefore there will be always large gaps in this time series. Also, during summer months the ice drift retrieval using AMSR-E data is hampered if not impossible due to melting conditions which cause a loss of the distinct surface features required for the maximum cross-correlation method. Thus for summer months our method would have to use alternative ice drift estimates.

We note that our approach of estimating sea ice volume transport is entirely satellite based and can therefore be applied to geographical regions other than the Greenland Sea. We anticipate that our method can easily be adapted to new freeboard measurements like the ones expected to be available from the upcoming CryoSat-II mission. CryoSat-II will measure continuously and thus the gaps in the time series could be significantly reduced by use of these data.

ACKNOWLEDGEMENTS

This work was supported by the German Research Foundation (DFG) project SFB 512-E1. The authors gratefully acknowledge the provision of ICESat and AMSR-E data by the National Snow and Ice Data Centre (NSIDC), Boulder, CO, USA. Especially we acknowledge the provision and support on sea ice drift data from AMSR-E data by Robert Ezraty and Fanny Ardhuin from IFREMER, Brest, France and the provision of the ArcGP geoid by Rene Forsberg from Danish National Space Centre, Copenhagen, Denmark.

REFERENCES

Aagaard, K. and E. Carmack, 1989: The role of sea ice and other fresh water in the Arctic Circulation, *J. Geophys. Res.*, 94(C10), 14,485-14,498.

Agnew, L., H. Le and T. Hirose, 1997: Estimation of large-scale sea ice motion from SSM/I 85.5 GHz imagery, *Ann. Glaciol.*, 25, 305-311.

Bamber, J.L. and A.J. Payne (*editors*), 2004: *The mass balance of the cryosphere : observations and modelling of contemporary and future changes*, Cambridge University Press, Cambridge, UK; New York.

Cavalieri, D.J., C.L. Parkinson and K. Y. Vinnikov, 2003: 30-year satellite record reveals contrasting Arctic and Antarctic decadal sea ice variability, *Geophys. Res. Lett.*, 30(18), L1970,

doi:10.1029/2003GL018031.
Cavalieri, D.J., C. Parkinson, P. Gloersen and H. Zwally, 2002: Sea ice concentrations from Nimbus-7 SMMR and DMSP SSM/I passive microwave data, *Tech. Rep., National Snow and Ice Data Center*, Boulder, Colorado, USA.
Comiso, J.C., D.J. Cavalieri and T. Markus, 2003: Sea ice concentration, ice temperature, and snow depth using AMSR-E data, *IEEE Trans. Geosci. Rem. Sens.*, 41, 243-252.
Dickson, R.R., J. Meincke, S.-A. Malmberg and A.J. Lee, 1988: The "Great Salinity Anomaly" in the northern North Atlantic 1968-1982, *Prog. Oceanogr.*, 20, 103-151.
Divine, D.V. and C. Dick, 2006: Historical variability of sea ice edge position in the Nordic Seas, *J. Geophys. Res.-Ocean*, 111, C01001.
Ezraty, R., F. Ardhuin and D. Croizé-Fillon, 2005: Sea ice drift in the Central Arctic using the 89 GHz brightness temperatures of the Advanced Microwave Scanning Radiometer (AMSR-E), *User's Manual, Version 1.0, Institut français de recherche pour l'exploitation de la mer (IFREMER), Brest, France*.
Forsberg, R. and H. Skourup, 2005: Arctic ocean gravity, geoid and sea-ice freeboard heights from ICESat and GRACE, *Geophys. Res. Lett.*, 32, L21502, doi: 1029/2005GL023711.
Forsberg, R. and S. Kenyon, 2004: Gravity and geoid in the Arctic region – The northern polar gap now filled. *Proceedings Second International GOCE Workshop "GOCE, The Geoid and Oceanography", ESA-ESRIN, Frascati, Italy, 8-10 March 2004*.
Haas, C., 2004: Late-summer sea ice thickness variability in the Arctic Transpolar Drift 1991-2001 derived from ground-based electromagnetic sounding, *Geophys. Res. Lett.*, 31, L09402, doi:10.1029/2003GL019394.
Hvidegård, S.M. and R. Forsberg, 2002: Sea-ice thickness from airborne laser altimetry over the Arctic Ocean north of Greenland, *Geophys. Res. Lett.*, 29(20), 1952-1955.
Johannessen, O.M., L. Bengtsson, M.W. Miles, S.I. Kuzmina, V.A. Semenov, G.V. Alekseev, A.P. Nagurnyi, V.F. Zakharov, L.P. Bobylev, L.H. Pettersson, K. Hasselmann and H.P. Cattle, 2004: Arctic climate change: observed and modeled temperature and sea-ice variability, *Tellus*, 56A(4), 328-341.
Kaleschke L., C. Lüpkes, T. Vihma, J. Haarpaintner, A. Bochert, J. Hartmann and G. Heygster, 2001: SSM/I sea ice remote sensing for mesoscale ocean-atmosphere interaction analysis, *Can. J. Rem. Sens.*, 27(5), 526-537.
Karstensen, J., P. Schlosser, D.W.R. Wallace, J.L. Bullister and J. Blindheim, 2005: Water mass transformation in the Greenland Sea during the 1990s, *J. Geophys. Res.*, 110, C07022, doi:10.1029/2004JC002510.
Kwok, R., G.F. Cunningham and S.S. Pang, 2004a: Fram Strait sea ice outflow, *J. Geophys. Res.*, 109, C01009, doi:10.1029/2003JC001785.
Kwok, R., H.J. Zwally and D. Yi, 2004b: ICESat observations of Arctic sea ice: A first look, *Geophys. Res. Lett.*, 31, L16401, doi:10.1029/2004GL020309.
Kwok, R., A. Schweiger, D.A. Rothrock, S. Pang and C. Kottmeier, 1998: Sea ice motion from satellite passive microwave imagery assessed with ERS SAR and buoy motions, *J. Geophys. Res.*, 103(C4), 8191-8214.
Laxon S., N. Peacock and D. Smith, 2003: High interannual variability of sea ice thickness in the Arctic region, *Nature*, 425, 947-950.
Pfirman S., W.F. Haxby, R. Colony and I. Rigor, 2004: Variability in Arctic sea ice drift, *Geophys. Res. Lett.*, 31, L16402, doi: 10.1029/ 2004GL020063.
Rothrock D. A., J. Zhang and Y. Yu, 2003: The Arctic ice thickness anomaly of the 1990s: A consistent view from observations and models, *J. Geophys. Res.*, 108, doi: 10.1029/2001JC001208.
Rothrock D. A., Y. Yu and G.A. Maykut, 1999: Thinning of the Arctic sea-ice cover, *Geophys. Res. Lett.*, 26(23), 3469-3472.
Spreen, G., S. Kern, D. Stammer, R. Forsberg and J. Haarpaintner, 2006: Satellite-based estimates of sea ice volume flux through Fram Strait, *Ann. Glaciol.*, 44, in press.
Spreen, G., S. Kern, R. Ezraty, H. Witte and D. Stammer, 2005a: Towards remote sensing of the net sea ice volume flux in the Greenland Sea, *Proc. 1st CryoSat Workshop, March 8-10, 2005, ESA ESRIN, Frascati, Italy,* http://earth.esa.int/workshops/cryosat2005/all.html.
Spreen, G., L. Kaleschke and G. Heygster, 2005b: Operational sea ice remote sensing with AMSR-E

89 GHz channels, *2005 IEEE International Geoscience and Remote Sensing Symposium Proceedings, Seoul, Korea, July 25—29*.
Vinje, T., N. Nordlund and A. Kvambekk, 1998: Monitoring ice thickness in the Fram Strait, *J. Geophys. Res.*, 103(C10), 10,437-10,449.
Wadhams, P., 2002: *Ice in the Ocean*, Gordon and Breach Science Publishers, London, 351pp.
Wadhams, P. and N. R. Davis, 2000: Further evidence of ice thinning in the Arctic Ocean, *Geophys. Res. Lett.*, 27, 3973-3975.
Warren, S.G., I.G. Rigor, N. Untersteiner, V.F. Radionov, N.N. Bryazgin, Y.I. Aleksandrov and R. Colony, 1999: Snow depth on Arctic sea ice, *J. Climate*, 12, 1814-1829.
Zwally, H.J., B. Schutz, W. Abdalati, J. Abshire, C. Bentley, A. Brenner, J. Bufton, J. Dezio, D. Hancock, D. Harding, T. Herring, B. Minster, K. Quinn, S. Palm, J. Spinhirne and R. Thomas, 2002: ICESat's laser measurements of polar ice, atmosphere, ocean, and land, *J. Geodyn*, 24, 405-445.